Applied Materials Today 2 (2016) 24–31

Contents lists available at ScienceDirect

Applied Materials Today

journal homepage: www.elsevier.com/locate/apmt

Novel hetero-bilayered materials for photovoltaics

Jia Zhou [a,b,*]

[a] Department of Chemistry, Harbin Institute of Technology, Harbin 150001, China
[b] Center for Nanophase Materials Sciences, Oak Ridge National Laboratory, Bethel Valley Road, Oak Ridge, TN 37831-6493, United States

ARTICLE INFO

Article history:
Received 13 October 2015
Received in revised form 4 December 2015
Accepted 7 December 2015

Keywords:
GaS
$MoSe_2$
Density functional theory
Two dimensional hetero-structures
Optical absorbance

ABSTRACT

The recently synthesized GaS and $MoSe_2$ nanosheets have been used as appropriate substrates for other layered materials, e.g. silicene/GaS heterosheets akin to graphene/BN systems. Here, we have performed a comprehensive first-principles study of the electronic and optical properties of two-dimensional (2D) GaS/$MoSe_2$ hetero-bilayers based on density functional theory (DFT). We found almost all proposed GaS/$MoSe_2$ hetero-bilayers in the current study have an indirect band gap from the Γ point to the K point, except for one with a direct band gap at the K point. Tunable band gaps GaS/$MoSe_2$ hetero-bilayers can be controlled by strain modulation. State-of-the-art *GW*-Bethe–Salpeter method, accounting for electron-electron and electron-hole interactions, has been employed to compute accurate absorbance spectra for layered materials. Compared with its composing GaS and $MoSe_2$ monolayers, GaS/$MoSe_2$ hetero-bilayers show superior behavior on optical absorbance, indicating a stronger visible-light absorption and applications in solar energy harvesting. We foresee that the novel GaS/$MoSe_2$ hetero-bilayers would stimulate the fabrication of materials with unprecedented optical and physico-chemical properties that may apply in nanodevices and photovoltaic cells.

1. Introduction

Graphene, a single atomic layer of graphite, has generated tremendous excitement since its discovery decade ago [1,2]. It also triggers a boom for other 2D layered materials. 2D layered materials such as graphene, hexagonal BN (h-BN), and transition metal chalcogenides (e.g. GaSe, GaS, $MoSe_2$, and WS_2) remain planar as separated simply by the mechanical [3] or liquid-phase exfoliation from their bulk layered solids [4]. The exfoliation is facilitated by the weak interlayer van der Waals (vdW) forces. These 2D layered materials have a broad range of applications, such as field-effect transistors, spin- or valley-tronics, thermoelectrics, topological insulators, and energy conversion and storage [5–8].

As a kind of layered semiconducting material, molybdenum dichalcogenides MoX_2 (X = S, Se) have attracted great interest due to a wide range of important properties [9–11]. The monolayer of $MoSe_2$ is composed of three sublayers stacked in the sequence Se–Mo–Se, as shown in Fig. 1c (MoS_2 is similar in structure). MoX_2 (X = S, Se) undergoes a crossover from indirect to direct gap when going from bilayer to monolayer [12], giving rise to enhanced monolayer luminescence [13], thus allowing applications such as transistors, photodetectors and electroluminescent devices [11]. On the other hand, layered gallium monochalcogenides GaX (X = S, Se) have also drawn much research attention for their potential applications in fields such as solar energy conversion [14]. Unlike MoX_2 monolayer, the monolayer of GaX consists of four sublayers stacked in the sequence X–Ga–Ga–X, as shown in Fig. 1a for GaS monolayer. Experimental efforts have since been carried out to fabricate these GaX in monolayer form, and monolayer GaS and GaSe sheets have already successfully been synthesized [15–18]. Soon after, theoretical calculations have also been undertaken to further understand the electronic and photonic properties of GaX monolayers [19,20]. The GaS monolayer applications in the experiments also include transistors and photodetectors [15–18].

Recently, the possibility to combine various 2D materials in vertical stacks creates a new paradigm in materials science: layered hetero-structures [21]. Those hetero-structures are upheld together by vdW interactions, and thus are called vdW hetero-structures. The hetero-structures have been widely used in conventional semi-conductors for achieving tunable electronic properties [12]. Graphene/h-BN vdW hetero-structures are one of the first research targets due to their commensurate structural parameters and distinct electronic properties, and a rich collection of physics and functionalities have been revealed by both experimental and theoretical investigations [22–26]. Moreover, a variety

* Correspondence to: Department of Chemistry, Harbin Institute of Technology, Harbin 150001, China.
E-mail address: jiazhou@hit.edu.cn

http://dx.doi.org/10.1016/j.apmt.2015.12.001
2352-9407/

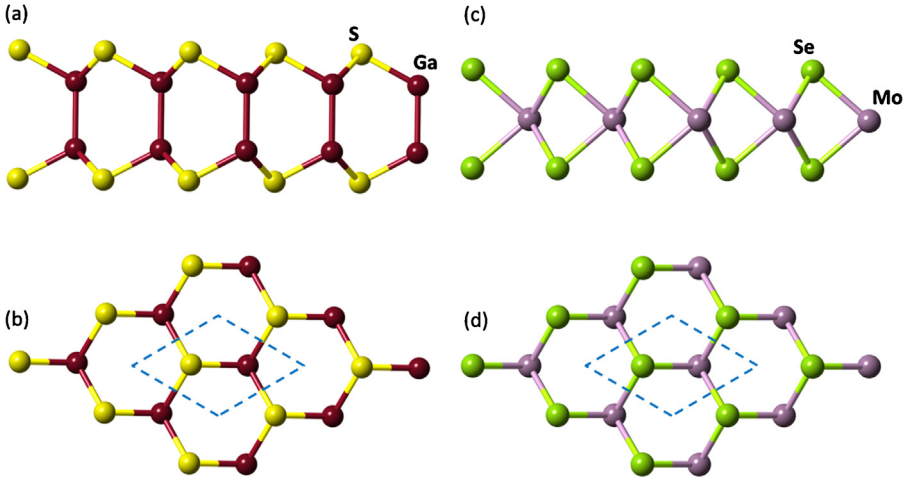

Fig. 1. Side view (a) and top view (b) of GaS monolayer with unit cell outlined; side view (c) and top view (d) of $MoSe_2$ monolayer with unit cell outlined.

of vdW hetero-structures involving molybdenum dichalcogenides MoX_2 (X = S, Se) [12,27–34] and GaS [35] have also been studied from both experimental and theoretical perspectives, such as silicene/GaS heterosheets and silicene/MoS_2 heterobilayers. It has been shown that MoX_2 and GaX (X = S, Se) are good substrates for other layered materials, such as graphene and silicene, or vise versa. The common ground of these vdW hetero-structures is that the in-plane lattice constants of the composing parts are comparable. From our own survey, GaS monolayer and $MoSe_2$ monolayer meet the above criterion. Given the individual excellent behavior of GaS monolayer and $MoSe_2$ monolayer on photoelectrochemistry, we wonder how the novel GaS/$MoSe_2$ hetero-bilayered materials will perform, in particular for photovoltaics, when GaS and $MoSe_2$ monolayers integrate into vdW hetero-bilayers.

In this work, we perform extensive first-principles calculations to characterize novel GaS/$MoSe_2$ hetero-bilayers, constructed by GaS and $MoSe_2$ monolayers. Electronic and optical properties of GaS/$MoSe_2$ hetero-bilayers are systematically investigated by both DFT and *GW*-Bethe–Salpeter method. Our work is expected to pave the way for a new generation of integrated devices and make hetero-bilayers viable candidates for electronic or photoelectrochemical applications.

2. Computational methods

First-principles calculations were carried out using the Vienna ab initio simulation package (VASP) [36,37]. The Kohn–Sham equations were solved using the projector-augmented wave (PAW) method [38,39]. For the structural relaxations, we employed the Perdew–Burke–Ernzerhof (PBE) functional [40,41] with the long-range dispersion correction implemented by Grimme [42]. The Brillouin-zone integrations were performed on a dense Γ-centered Monkhorst-Pack $16 \times 16 \times 1$ k-point grid [43]. The kinetic energy cutoff for plane waves was set to 500 eV and the "accurate" precision setting was adopted to avoid wrap around errors. The convergence criterion for the electronic self-consistent loop was set to 10^{-5} eV. During the structural relaxations, the vacuum regions were at least 20 Å to ensure the periodic images are well separated while other lattice vectors were fully relaxed. All atoms were also relaxed until the Hellmann–Feynman forces were smaller than 0.01 eV/Å.

The electron-hole interaction plays an important role in the optical response of a material [44]. We calculated the optical spectra of layered materials, including the excitonic interaction, by solving the Bethe–Salpeter equation (BSE), which is implemented in the VASP [45,46]. The BSE spectrum calculations started with the single-shot G_0W_0 quasiparticle energies and the PBE wave functions. For the more expensive G_0W_0 and BSE calculations, a $12 \times 12 \times 1$ k-point grid was applied, which is mostly sufficient for proper description of excitons [47]. The energy cutoff for the response function was set to 150 eV, and the particular pseudopotentials provided in VASP for *GW* calculations (e.g. Mo_sv_GW PAW potential accounting of $4s^2 4p^6 4d^5 5s^1$ valence electrons for Mo) were used for the G_0W_0 and BSE calculations. A total of 96 bands (more than 4 times of the number of occupied bands in almost all cases ensuring the accuracy of the results) and 96 frequency points were included in the G_0W_0 calculations, which were followed by the BSE calculations. The seven highest valence and seven lowest conduction bands were included in the calculation of the excitonic states for monolayers, while fourteen highest valence and fourteen lowest conduction bands were included for bilayers. Spin-orbit effect at the *GW* level was within a few tens of meVs, as indicated in the previous study of similar systems [48], and was omitted here for sake of computational costs. The adopted computational methodology for G_0W_0 and BSE calculations has been validated in our previous work [49] and others [20,29,33,34,48] for similar individual monolayer sheets. This approach balances the accuracy and computational costs of our results, and we expect the general trends predicted in this study to be robust.

3. Results and discussion

For reference, we first study the structures of GaS and $MoSe_2$ monolayers, as shown in Fig. 1. Both of them have a same symmetry as graphene. The calculated lattice constants are 3.58 Å and 3.32 Å for GaS and $MoSe_2$ monolayers, respectively. These values agree well with previous studies of GaS and $MoSe_2$ [9,20,50]. The closely-matched lattice parameters of GaS and $MoSe_2$ monolayers make them possible candidates to form hetero-bilayered structure, as seen in Fig. 2c, without significantly high strain (GaS [19] and $MoSe_2$ [12] monolayers have been studied already with strain up to 10% and 8%, respectively). For comparison, GaS/GaS and $MoSe_2$/$MoSe_2$ bilayers have also been investigated, which are shown in Fig. 2a and b. GaS bulk favors the β structure, which is AB stacking [51]. Previous studies of layered transition-metal dichalcogenides (e.g. MoS_2, $MoSe_2$, and WSe_2) show that only AB stacking, also called C7 stacking [27], gives rise to the lowest energy in most hetero-bilayer systems, and electronic structure is quite insensitive to the stacking [12,27]. Therefore, for all the bilayers in our current work, the two layers are arranged with AB stacking,

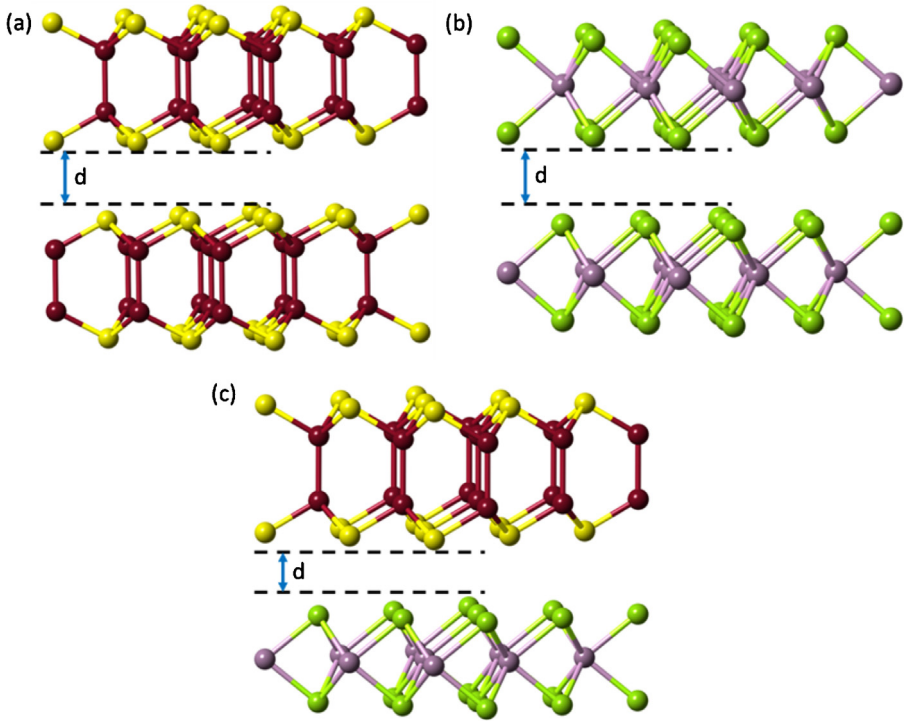

Fig. 2. GaS/GaS bilayer (a), $MoSe_2$/$MoSe_2$ bilayer (b), and GaS/$MoSe_2$ hetero-bilayer (c).

so-called C7 stacking. The distances (d in Fig. 2) between layers are 3.178 Å, 3.203 Å, and 3.113 Å for fully optimized GaS/GaS bilayer, $MoSe_2$/$MoSe_2$ bilayer, and GaS/$MoSe_2$ hetero-bilayer, respectively. The closer layer-layer distance in GaS/$MoSe_2$ hetero-bilayer than GaS/GaS bilayer and $MoSe_2$/$MoSe_2$ bilayer, as well as the negative interaction energy (−0.17 eV), indicates at least comparable interaction, if not stronger, between GaS monolayer and $MoSe_2$ monolayer, and thus could be made in the experiments.

Before we discuss the electronic properties of GaS/$MoSe_2$ hetero-bilayer, we first study the electronic properties of GaS and $MoSe_2$ monolayers and their respective homo-bilayers. Fig. 3 shows the band structures of GaS and $MoSe_2$ monolayers, as well as GaS/GaS and $MoSe_2$/$MoSe_2$ bilayers. Only $MoSe_2$ monolayer has a direct band gap at the K point, while all the other three have an indirect band gap. For $MoSe_2$/$MoSe_2$ bilayer, the valence band maximum (VBM) relocates to the Γ point and the conduction band minimum (CBM) moves somewhere between the Γ and K points, compared with $MoSe_2$ monolayer. For GaS monolayer and GaS/GaS bilayer, the CBM is at the M point, while the VBM is between the Γ and M points. The band gaps are calculated by both PBE and G_0W_0, and are collected in Table 1. These values are in good accord with the previous studies [12,19,20,33,48,50], validating the accuracy of our approach. It is well-known that the PBE functional usually underestimates the band gaps [52], while quasiparticle *GW* calculation could generally correct them. For GaS monolayer and GaS/GaS bilayer, G_0W_0 band gaps are 1.2–1.5 eV over PBE band gaps, while for $MoSe_2$ monolayer and $MoSe_2$/$MoSe_2$ bilayer, G_0W_0 band gaps are only 0.5–0.8 eV over PBE. It is interesting to note that for GaS monolayer and bilayer, PBE suggests they are both semiconductors with a band gap below 3 eV, while G_0W_0 indicates they are insulators with a band gap over 3 eV. Since there is no experimental bandgap data for GaS monolayer and bilayer and in some cases *GW* method overestimates the band gaps [9], we only can conclude that the exact band gaps of GaS monolayer and bilayer, should be between PBE and G_0W_0 values. On the other hand, $MoSe_2$ monolayer and bilayer are semiconductors by both PBE and G_0W_0.

Table 1
Band Gaps (E_g in eV) for layered materials, and positions of **a** (first peak of the spectrum) and **b** (the highest peak within the range of visible light in the spectrum) (in eV) in BSE optical spectra.

	E_g (PBE/G_0W_0)	**a**	**b**
GaS monolayer	2.57/4.03	3.74	
GaS/GaS bilayer	2.14/3.32	3.76	
$MoSe_2$ monolayer	1.45/2.22	1.69	2.36
$MoSe_2$/$MoSe_2$ bilayer	1.21/1.71	1.73	2.72
GaS/$MoSe_2$ hetero-bilayer with different strains (ε)	E_g (PBE/G_0W_0)	**a**	**b**
−4%	1.17/1.19	1.74	2.48
−3%	1.28/1.71	1.57	2.49
−1%	0.87/1.64	1.36	2.42
0%	0.79/1.55	1.31	2.38
1%	0.53/1.26	1.19	2.26
3%	0.26/0.96	1.05	2.15

GaS monolayer has a distinct electronic property from $MoSe_2$ monolayer, e.g. much larger band gap (the difference is over 1.5 eV by G_0W_0). However, GaS and $MoSe_2$ monolayers are close in lattice. It would be interesting to investigate the electronic properties of GaS/$MoSe_2$ hetero-bilayers. At first, we fully relaxed the whole GaS/$MoSe_2$ hetero-bilayer, and obtained the most stable hetero-bilayered structure with a lattice constant 3.45 Å, lying in the middle of those of GaS and $MoSe_2$ monolayers. Strain modulation has been commonly used in low-dimensional systems to finely tune their electronic properties. Fig. 4 shows the band structures of various GaS/$MoSe_2$ hetero-bilayers, with different in-plane strains (positive strains indicate tension while negative strains denote compression). Relative to the most stable GaS/$MoSe_2$ hetero-bilayer, the strain (ε) of various GaS/$MoSe_2$ hetero-bilayers is from −4% (the in-plane lattice constant is the same as pristine $MoSe_2$ monolayer) to 3% (the in-plane lattice constant is the same as pristine GaS monolayer). All the band structures show an indirect band gap, except for that of lattice constant of $MoSe_2$ monolayer in Fig. 4a. The band gap of GaS/$MoSe_2$ hetero-bilayer with −4% strain

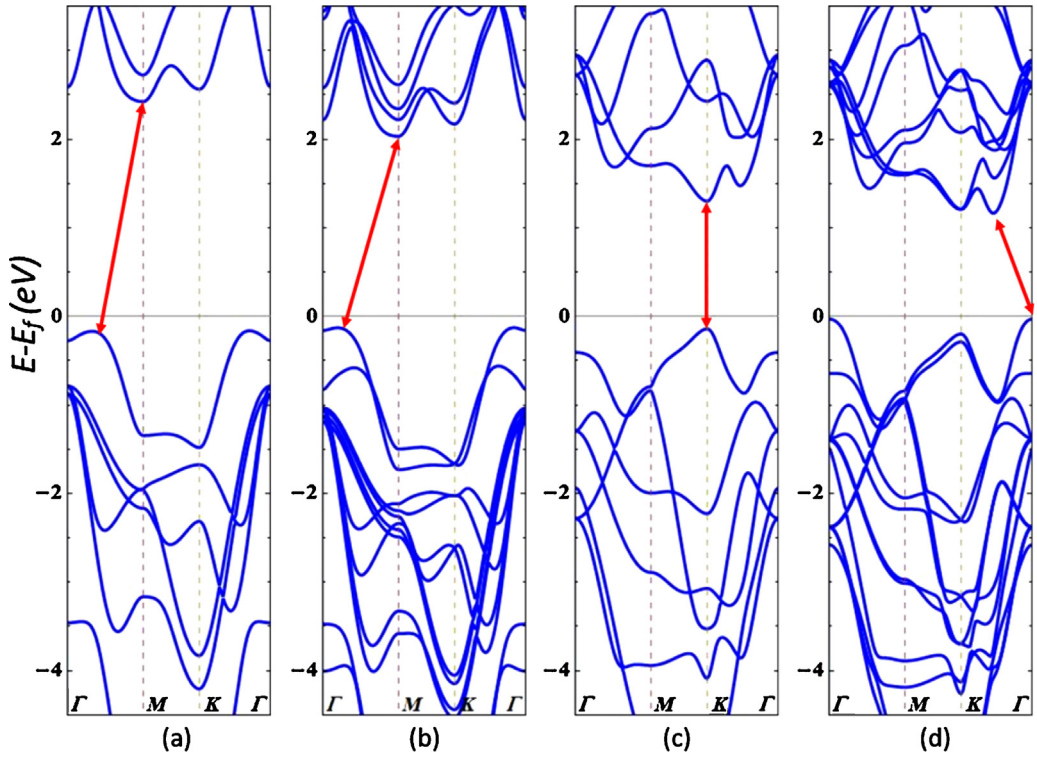

Fig. 3. Band structures of GaS monolayer (a), GaS/GaS bilayer (b), $MoSe_2$ monolayer (c), and $MoSe_2$/$MoSe_2$ bilayer (d). The red solid arrows indicate the band gap. (For interpretation of the references to color in this figure legend, the reader is referred to the web version of this article.)

is 1.17/1.19 eV by PBE/G_0W_0 at the K point, which is significantly decreased compared with that of $MoSe_2$ monolayer (1.45/2.22 eV by PBE/G_0W_0). The CBM of other hetero-bilayers remains at the K point, while the VBM shifts to the Γ point. Judging the band structures, it is clear that the highest valence band and the lowest conduction band of hetero-bilayers both come from $MoSe_2$ monolayer, and the VBM shift the K point to the Γ point was also observed in the pristine $MoSe_2$ monolayer with tensile biaxial strains [53]. The band gaps for all GaS/$MoSe_2$ hetero-bilayers are collected in Table 1 as well. The band gap reaches the peak at 1.28/1.71 eV by PBE/G_0W_0 in Fig. 4b, and then deceases monotonously when the in-plane lattice constant growing.

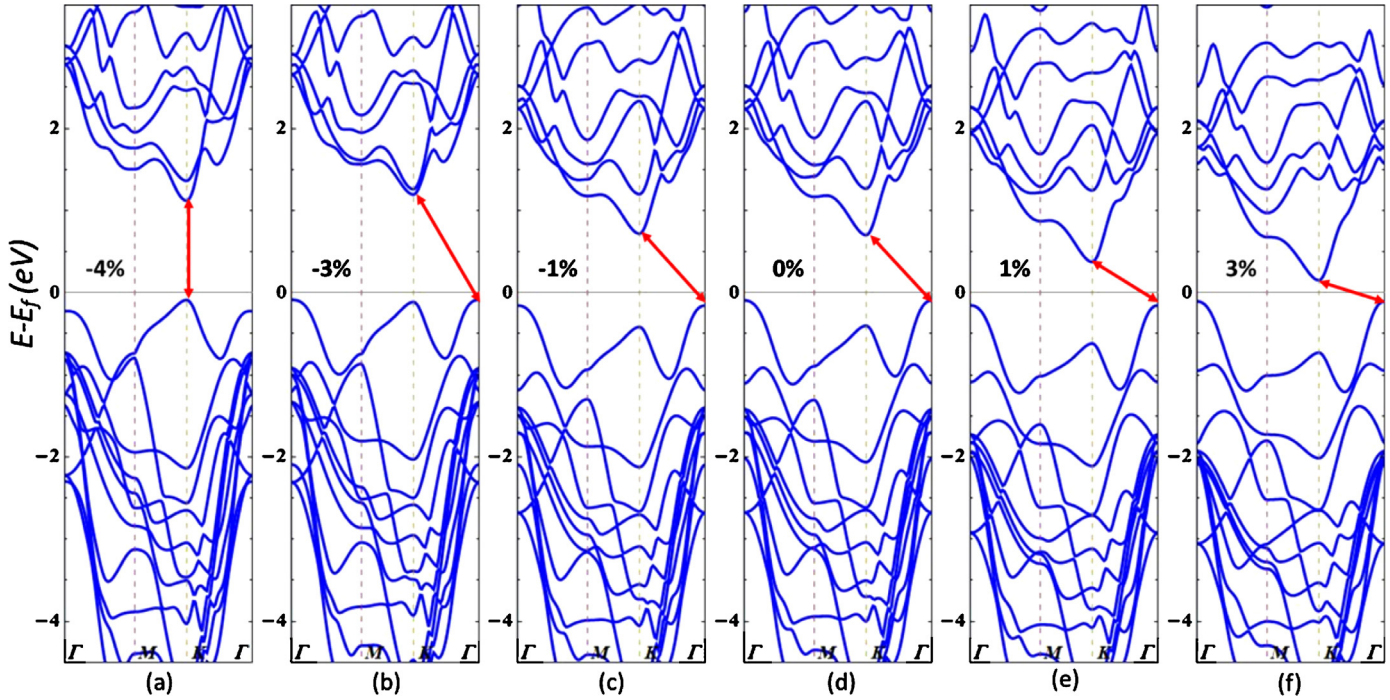

Fig. 4. Band structures of GaS/$MoSe_2$ hetero-bilayers with different strains: (a) −4%, (b) −3%, (c) −1%, (d) 0%, (e) 1%, and (f) 3%. The red solid arrows indicate the band gap. (For interpretation of the references to color in this figure legend, the reader is referred to the web version of this article.)

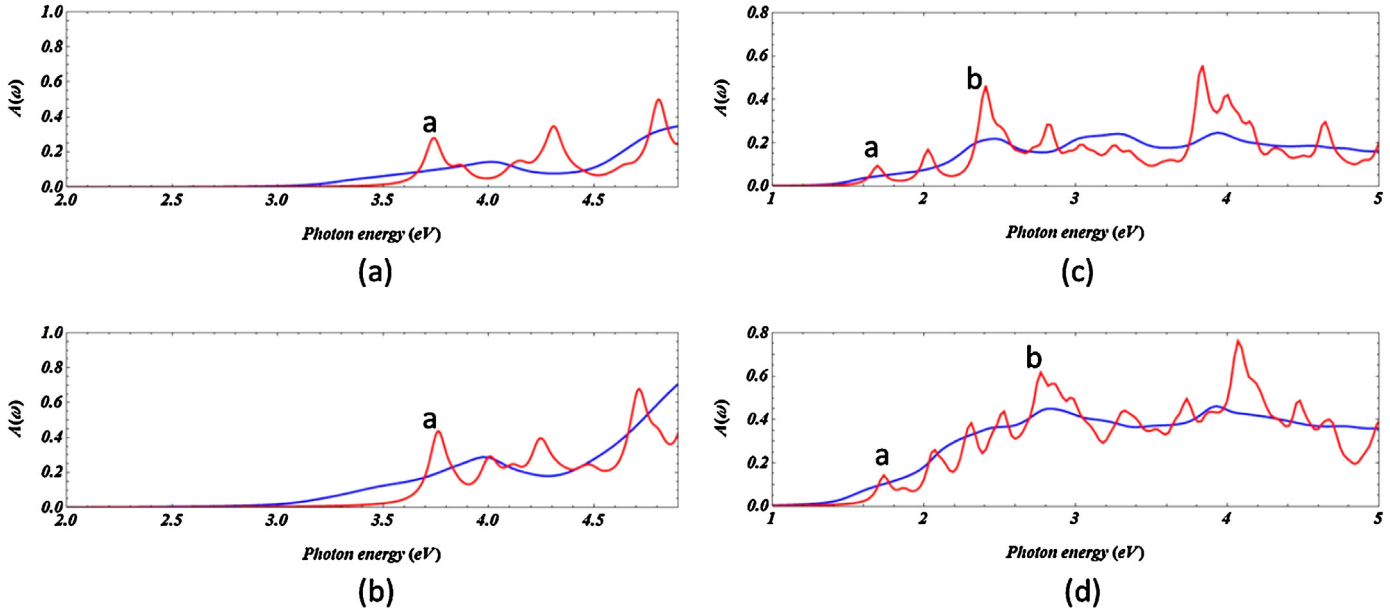

Fig. 5. Optical absorbance spectra $A(\omega)$ (red: GW_BSE; blue: RPA) of GaS monolayer (a), GaS/GaS bilayer (b), $MoSe_2$ monolayer (c), and $MoSe_2/MoSe_2$ bilayer (d). Label a indicates the first peak of GW_BSE curves, while label b indicates the highest peak of GW_BSE curves below 3.26 eV. (For interpretation of the references to color in this figure legend, the reader is referred to the web version of this article.)

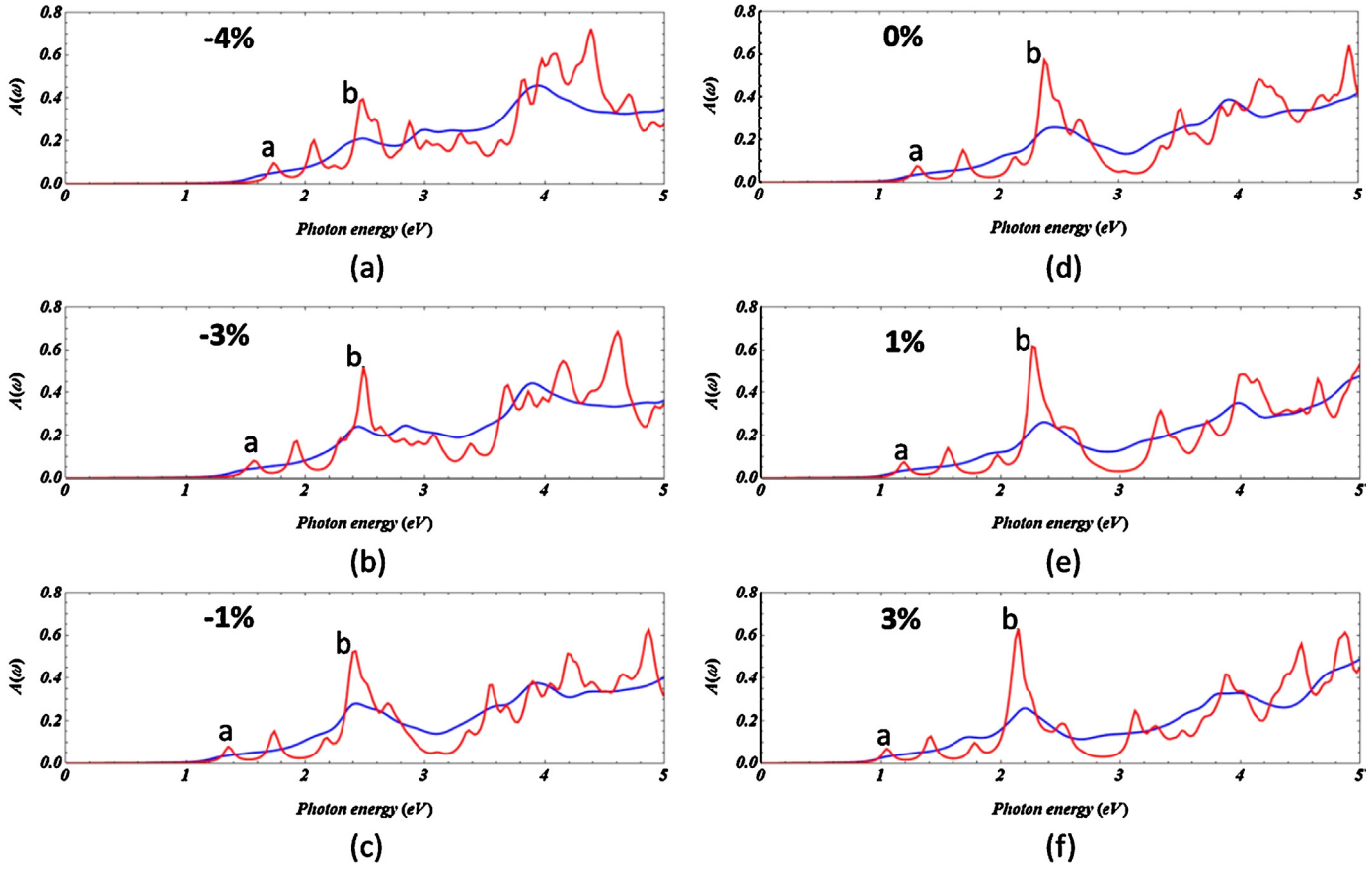

Fig. 6. Optical absorbance spectra $A(\omega)$ (red: GW_BSE; blue: RPA) of $GaS/MoSe_2$ hetero-bilayers with different strains: (a) −4%, (b) −3%, (c) −1%, (d) 0%, (e) 1%, and (f) 3%. Label a indicates the first peak of GW_BSE curves, while label b indicates the highest peak of GW_BSE curves below 3.26 eV. (For interpretation of the references to color in this figure legend, the reader is referred to the web version of this article.)

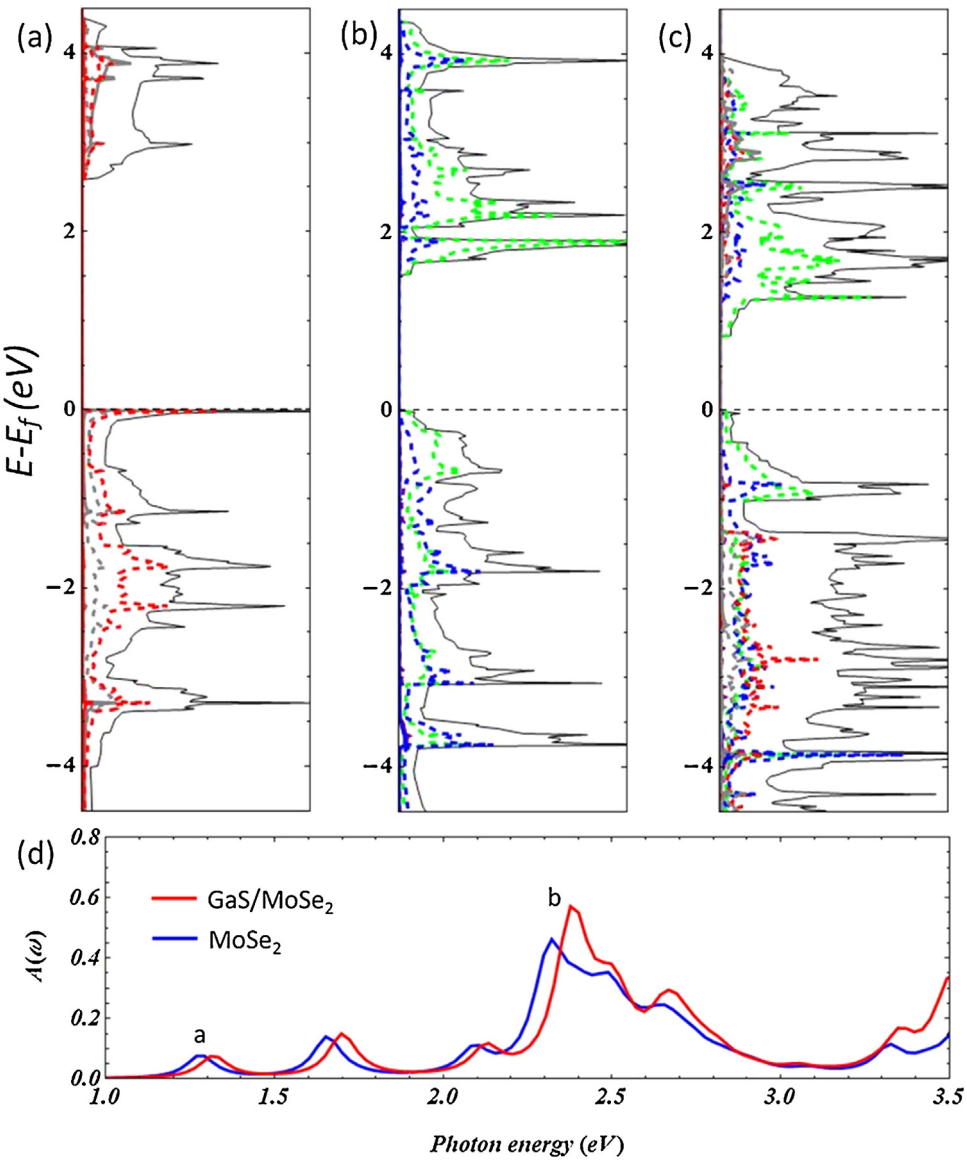

Fig. 7. Total/partial DOS of GaS monolayer (a), $MoSe_2$ monolayer (b), and GaS/$MoSe_2$ hetero-bilayer (c) (black: total DOS; solid gray: Ga-s pDOS; dashed gray: Ga-p pDOS; solid red: S-s pDOS; dashed red: S-p pDOS; solid purple: Mo-s pDOS; dashed purple: Mo-p pDOS; dashed green: Mo-d pDOS; solid blue: Se-s pDOS; dashed blue: Se-p pDOS). (d) Optical absorbance spectra $A(\omega)$ of the most stable GaS/$MoSe_2$ hetero-bilayer (red) and of its composing $MoSe_2$ monolayer (blue), computed using BSE. (For interpretation of the references to color in this figure legend, the reader is referred to the web version of this article.)

Next we turn to an important optical property of various GaS/$MoSe_2$ hetero-bilayers: optical absorbance $A(\omega)$, defined as the fraction of photons of energy $E = \hbar\omega$ absorbed by the 2D sheets. For light with a polarization vector within the plane of the 2D sheet, $A(\omega)$ is calculated by $A(\omega) = \omega \times L \times \varepsilon_2/c$, where ω is the frequency of photon, L is the interlayer spacing between the isolated layers, ε_2 is the imaginary part of the dielectric function, and c is the speed of light in vacuum [54]. The imaginary part of the dielectric function is calculated by solving the BSE and random-phase approximation (RPA), respectively. Since RPA ignores the electron-hole interaction, its results are not as accurate as those of BSE, and they are shown along with BSE only for the comparison purpose. For comparison, we first study the absorption spectra of GaS and $MoSe_2$ monolayers, as well as GaS/GaS and $MoSe_2$/$MoSe_2$ bilayers, as shown in Fig. 5. It is clear that GaS monolayer and bilayer have no absorption below 3.26 eV, which is the range of visible light. The first peak of the spectrum (peak **a**, which is used hereafter) is 3.74 eV and 3.76 eV for GaS monolayer and bilayer, respectively. By contrast, the first peaks of $MoSe_2$ monolayer and bilayer are well below 2.0 eV. Our calculated exciton binding energy (the energy difference between the band gap and peak **a**) of $MoSe_2$ monolayer (0.53 eV) agrees well with the previous calculation [33,48]. Furthermore, the highest absorption of $MoSe_2$ within the range of visible light (1.65–3.26 eV) occurs at 2.36 eV (peak **b**, which is used hereafter) for monolayer, and 2.72 eV (peak **b**) for bilayer. The positions of peak **a** and **b** are collected in Table 1. The absorption at the peak **b** is over 40% and 60% for $MoSe_2$ monolayer and bilayer, respectively.

Fig. 6 shows the absorption spectra of various GaS/$MoSe_2$ hetero-bilayers in accord with Fig. 4. The positions of peak **a** and **b** are collected in Table 1 as well. The position of peak **a** decreases from 1.74 eV (Fig. 6a) to 1.05 eV (Fig. 6f) with the increase of the lattice constant. The position of peak **b** reaches the peak at 2.49 eV (Fig. 6b), and goes downhill gradually afterwards. On the other hand, it would be crucial to compare the height of peak **b**, because it is directly related to the optical absorbance capacity of different 2D layered materials within the range of visible light. From Fig. 5, GaS monolayer and bilayer have no obvious absorption in the range of visible light, while $A(\omega)$ values of peak **b** are 0.47 and 0.61

for $MoSe_2$ monolayer and bilayer, respectively. As for GaS/$MoSe_2$ hetero-bilayers, $A(\omega)$ value of peak **b** increases from 0.40 (Fig. 6a) to 0.64 (Fig. 6f) with the increase of the in-plane lattice constant. The $A(\omega)$ value of peak **b** of the most stable GaS/$MoSe_2$ hetero-bilayer (Fig. 6d) is 0.57, just slightly lower than that of $MoSe_2$ bilayer. However, peak **b** in Fig. 6d is much sharper than its counterpart in Fig. 5d, indicating a much more selective absorption behavior of the light of certain wavelength.

In order to know the detailed contribution from individual layers of GaS/$MoSe_2$ hetero-bilayer, we study the density of states (DOS) of GaS monolayer, $MoSe_2$ monolayer, and GaS/$MoSe_2$ hetero-bilayer, as shown in Fig. 7a–c. For GaS monolayer, it can be seen that the valence bands from −2 to 0 eV are dominated mainly by S's p state and Ga's p state. On the other hand, the conduction bands from 2 to 4 eV consist mainly of the hybridization from Ga's s and S's p states. For $MoSe_2$ monolayer, however, both the valence bands and the conduction bands within the range from −2 to 4 eV are dominated by Se's p state and Mo's d state. When stacking into GaS/$MoSe_2$ hetero-bilayer, Mo's d state and Se's p state from $MoSe_2$ are still dominant in both the valence bands and the conduction bands. However, the components from GaS are outnumbered significantly by those from $MoSe_2$ near the Fermi level. Also as mentioned previously, GaS monolayer has no absorption below 3.26 eV, while $MoSe_2$ monolayer does. That raises the question if the optical absorbance of GaS/$MoSe_2$ hetero-bilayer mainly comes from the $MoSe_2$ part, only with some structural strain from its free monolayer. Fig. 7d shows optical absorbance spectra $A(\omega)$ of most stable GaS/$MoSe_2$ hetero-bilayer and of its composing $MoSe_2$ monolayer (directly taken from GaS/$MoSe_2$ hetero-bilayer), computed by BSE. It is clear that the absorbance spectrum of GaS/$MoSe_2$ hetero-bilayer is blue shift compared with that of its composing $MoSe_2$ monolayer. Furthermore, the peak **b** of GaS/$MoSe_2$ hetero-bilayer is 0.57 compared with 0.46 (very close to 0.47 of free $MoSe_2$ monolayer itself) of the composing $MoSe_2$ monolayer. It is almost a quarter increase of the optical absorbance of $MoSe_2$ monolayer, indicating a significantly positive contribution from GaS monolayer, not by structural strain from free $MoSe_2$ monolayer itself.

4. Conclusion

In summary, we have investigated the electronic and optical properties of various GaS/$MoSe_2$ hetero-bilayers by DFT and state-of-the-art many-body perturbation theory including quasiparticle *GW* approach and BSE. Even though GaS monolayer has a distinct electronic property from $MoSe_2$ monolayer, they have the same symmetry with close lattice constants, making them good candidates to form GaS/$MoSe_2$ hetero-bilayers. Most GaS/$MoSe_2$ hetero-bilayers in our current study have an indirect band gap from the Γ point to the K point. With respect to the optical absorbance, GaS/$MoSe_2$ hetero-bilayers show superior behavior compared with its composing GaS and $MoSe_2$ monolayers. These theoretical predictions suggest that GaS/$MoSe_2$ hetero-bilayers might be very promising for optoelectronic applications at the nanometer scale.

Competing financial interests

The author declares no competing financial interests.

Acknowledgements

This research is supported by the Fundamental Research Funds for the Central Universities of China (Grant No. AUGA5710013115). This work used computational resources of the Oak Ridge Leadership Computing Facility at Oak Ridge National laboratory and of the National Energy Research Scientific Computing Center, which are supported by the Office of Science of the U.S. Department of Energy under Contract No. DE-AC05-00OR22750 and DE-AC02-05CH11231, respectively. We acknowledge the support from the Center for Nanophase Materials Sciences, which is sponsored at ORNL by the Scientific User Facilities Division, U.S. Department of Energy. The author also thanks Dr. Jingsong Huang (ORNL, US) and Prof. Xiaoming Cao (ECUST, China) for the assistance on the computations.

References

[1] K.S. Novoselov, A.K. Geim, S.V. Morozov, D. Jiang, Y. Zhang, S.V. Dubonos, I.V. Grigorieva, A.A. Firsov, Science 306 (2004) 666–669.
[2] K.S. Novoselov, A.K. Geim, S.V. Morozov, D. Jiang, M.I. Katsnelson, I.V. Grigorieva, S.V. Dubonos, A.A. Firsov, Nature 438 (2005) 197–200.
[3] K.S. Novoselov, D. Jiang, F. Schedin, T.J. Booth, V.V. Khotkevich, S.V. Morozov, A.K. Geim, Proc. Natl. Acad. Sci. U. S. A. 102 (2005) 10451–10453.
[4] J.N. Coleman, M. Lotya, A. O'Neill, S.D. Bergin, P.J. King, U. Khan, K. Young, A. Gaucher, S. De, R.J. Smith, I.V. Shvets, S.K. Arora, G. Stanton, H.-Y. Kim, K. Lee, G.T. Kim, G.S. Duesberg, T. Hallam, J.J. Boland, J.J. Wang, J.F. Donegan, J.C. Grunlan, G. Moriarty, A. Shmeliov, R.J. Nicholls, J.M. Perkins, E.M. Grieveson, K. Theuwissen, D.W. McComb, P.D. Nellist, V. Nicolosi, Science 331 (2011) 568–571.
[5] S.Z. Butler, S.M. Hollen, L. Cao, Y. Cui, J.A. Gupta, H.R. Gutiérrez, T.F. Heinz, S.S. Hong, J. Huang, A.F. Ismach, E. Johnston-Halperin, M. Kuno, V.V. Plashnitsa, R.D. Robinson, R.S. Ruoff, S. Salahuddin, J. Shan, L. Shi, M.G. Spencer, M. Terrones, W. Windl, J.E. Goldberger, ACS Nano 7 (2013) 2898–2926.
[6] C.N.R. Rao, H.S.S. Ramakrishna Matte, U. Maitra, Angew. Chem. Int. 52 (2013) 13162–13185.
[7] Q. Tang, Z. Zhou, Prog. Mater. Sci. 58 (2013) 1244–1315.
[8] P. Miro, M. Audiffred, T. Heine, Chem. Soc. Rev. 43 (2014) 6537–6554.
[9] C. Ataca, H. Şahin, S. Ciraci, J. Phys. Chem. C 116 (2012) 8983–8999.
[10] W.S. Yun, S.W. Han, S.C. Hong, I.G. Kim, J.D. Lee, Phys. Rev. B 85 (2012) 033305.
[11] Q.H. Wang, K. Kalantar-Zadeh, A. Kis, J.N. Coleman, M.S. Strano, Nat Nano 7 (2012) 699–712.
[12] N. Lu, H. Guo, L. Li, J. Dai, L. Wang, W.-N. Mei, X. Wu, X.C. Zeng, Nanoscale 6 (2014) 2879–2886.
[13] S. Tongay, J. Zhou, C. Ataca, K. Lo, T.S. Matthews, J. Li, J.C. Grossman, J. Wu, Nano Lett. 12 (2012) 5576–5580.
[14] A. Aruchamy, Photoelectrochemistry and Photovoltaics of Layered Semiconductors, Springer, 1992.
[15] P. Hu, Z. Wen, L. Wang, P. Tan, K. Xiao, ACS Nano 6 (2012) 5988–5994.
[16] D.J. Late, B. Liu, J. Luo, A. Yan, H.S.S.R. Matte, M. Grayson, C.N.R. Rao, V.P. Dravid, Adv. Mater. 24 (2012) 3549–3554.
[17] D.J. Late, B. Liu, H.S.S.R. Matte, C.N.R. Rao, V.P. Dravid, Adv. Funct. Mater. 22 (2012) 1894–1905.
[18] S. Lei, L. Ge, Z. Liu, S. Najmaei, G. Shi, G. You, J. Lou, R. Vajtai, P.M. Ajayan, Nano Lett. 13 (2013) 2777–2781.
[19] Y. Ma, Y. Dai, M. Guo, L. Yu, B. Huang, Phys. Chem. Chem. Phys. 15 (2013) 7098–7105.
[20] H.L. Zhuang, R.G. Hennig, Chem. Mater. 25 (2013) 3232–3238.
[21] L. Britnell, R.M. Ribeiro, A. Eckmann, R. Jalil, B.D. Belle, A. Mishchenko, Y.-J. Kim, R.V. Gorbachev, T. Georgiou, S.V. Morozov, A.N. Grigorenko, A.K. Geim, C. Casiraghi, A.H.C. Neto, K.S. Novoselov, Science 340 (2013) 1311–1314.
[22] C.R. Dean, A.F. Young, I. Meric, C. Lee, L. Wang, S. Sorgenfrei, K. Watanabe, T. Taniguchi, P. Kim, K.L. Shepard, J. Hone, Nat. Nanotech. 5 (2010) 722–726.
[23] Y. Fan, M. Zhao, Z. Wang, X. Zhang, H. Zhang, Appl. Phys. Lett. 98 (2011) 083103.
[24] J. Xue, J. Sanchez-Yamagishi, D. Bulmash, P. Jacquod, A. Deshpande, K. Watanabe, T. Taniguchi, P. Jarillo-Herrero, B.J. LeRoy, Nat. Mater. 10 (2011) 282–285.
[25] M. Yankowitz, J. Xue, D. Cormode, J.D. Sanchez-Yamagishi, K. Watanabe, T. Taniguchi, P. Jarillo-Herrero, P. Jacquod, B.J. LeRoy, Nat. Phys. 8 (2012) 382–386.
[26] W. Yang, G. Chen, Z. Shi, C.-C. Liu, L. Zhang, G. Xie, M. Cheng, D. Wang, R. Yang, D. Shi, K. Watanabe, T. Taniguchi, Y. Yao, Y. Zhang, G. Zhang, Nat. Mater. 12 (2013) 792–797.
[27] K. Kośmider, J. Fernández-Rossier, Phys. Rev. B 87 (2013) 075451.
[28] H. Terrones, F. López-Urías, M. Terrones, Sci. Rep. 3 (2013) 1549.
[29] M. Bernardi, M. Palummo, J.C. Grossman, Nano Lett. 13 (2013) 3664–3670.
[30] X. Li, Y. Dai, Y. Ma, Q. Liu, B. Huang, Nanotechnology 26 (2015) 135703.
[31] N. Gao, J.C. Li, Q. Jiang, Phys. Chem. Chem. Phys. 16 (2014) 11673.
[32] D. Chiappe, E. Scalise, E. Cinquanta, C. Grazianetti, B. van den Broek, M. Fanciulli, M. Houssa, A. Molle, Adv. Mater. 26 (2014) 2096–2101.
[33] M.M. Ugeda, A.J. Bradley, S.-F. Shi, F.H. da Jornada, Y. Zhang, D.Y. Qiu, W. Ruan, S.-K. Mo, Z. Hussain, Z.-X. Shen, F. Wang, S.G. Louie, M.F. Crommie, Nat. Mater. 13 (2014) 1091–1095.
[34] H.-P. Komsa, A.V. Krasheninnikov, Phys. Rev. B 88 (2013) 085318.
[35] Y. Ding, Y. Wang, Appl. Phys. Lett. 103 (2013) 043114.
[36] G. Kresse, J. Furthmüller, Phys. Rev. B 54 (1996) 11169–11186.
[37] M. Shishkin, G. Kresse, Phys. Rev. B 74 (2006) 035101.
[38] P.E. Blöchl, Phys. Rev. B 50 (1994) 17953–17979.
[39] G. Kresse, D. Joubert, Phys. Rev. B 59 (1999) 1758–1775.

[40] J.P. Perdew, K. Burke, M. Ernzerhof, Phys. Rev. Lett. 77 (1996) 3865–3868.
[41] J.P. Perdew, K. Burke, M. Ernzerhof, Phys. Rev. Lett. 78 (1997) 1396.
[42] S. Grimme, J. Comput. Chem. 27 (2006) 1787–1799.
[43] H.J. Monkhorst, J.D. Pack, Phys. Rev. B 13 (1976) 5188–5192.
[44] G. Onida, L. Reining, A. Rubio, Rev. Mod. Phys. 74 (2002) 601–659.
[45] P. Rinke, A. Schleife, E. Kioupakis, A. Janotti, C. Rödl, F. Bechstedt, M. Scheffler, C.G. Van de Walle, Phys. Rev. Lett. 108 (2012) 126404.
[46] C. Rödl, F. Bechstedt, Phys. Rev. B 86 (2012) 235122.
[47] A. Molina-Sánchez, D. Sangalli, K. Hummer, A. Marini, L. Wirtz, Phys. Rev. B 88 (2013) 045412.
[48] H.-P. Komsa, A.V. Krasheninnikov, Phys. Rev. B 86 (2012) 241201.
[49] J. Zhou, B.G. Sumpter, P.R.C. Kent, J. Huang, ACS Appl. Mater. Interfaces 7 (2015) 1458–1464.
[50] W. Huang, H. Da, G. Liang, J. Appl. Phys. 113 (2013) 104304.
[51] Z. Zhu, Y. Cheng, U. Schwingenschlögl, Phys. Rev. Lett. 108 (2012) 266805.
[52] J.P. Perdew, Int. J. Quantum Chem. 28 (1985) 497–523.
[53] C.-H. Chang, X. Fan, S.-H. Lin, J.-L. Kuo, Phys. Rev. B 88 (2013) 195420.
[54] L. Yang, J. Deslippe, C.-H. Park, M.L. Cohen, S.G. Louie, Phys. Rev. Lett. 103 (2009) 186802.